Progress In Electromagnetics Research M, Vol. 117, 13–23, 2023

Phase Gradient Metasurface Assisted Wideband Circularly Polarized Monopole Antenna

Punneth K. Tharehalli Rajanna[1, *], Krishnamoorthy Kanadasamy[2], and Pratik Meveda[3]

Abstract—An asymmetric coplanar waveguide (CPW) fed wideband circularly polarized monopole antenna with a slot structure is proposed in this article. Phase gradient metasurface (PGM) is placed beneath the monopole to improve the gain. Circular polarization (CP) is achieved over wide bandwidth by combining the monopole and slot modes. The asymmetric CPW-fed monopole antenna provides CP at lower frequencies, and slot mode provides CP at higher frequencies. The asymmetric ground plane in the monopole and asymmetric strips in the slot are combined to produce wide axial ratio bandwidth. The proposed design's detailed construction and operation are discussed with experimental validation. The proposed wideband CP antenna provides an impedance bandwidth of 95.46% and axial ratio bandwidth of 67.61%. The peak gain of 5.2 dBic is obtained at 2.35 GHz with 2 dB variation over operating bandwidth. The obtained radiation patterns provide good broadside radiation with better cross-polarization levels than co-polarization.

1. INTRODUCTION

Nowadays, wireless communication has grown extensively due to the increased use of wireless devices. The devices need to receive a good amount of power from the receiver for effective communication. Antennas play a significant role in receiving and transmitting waves. Circularly polarized antennas are more popular due to their advantages over linearly polarized antennas. Circularly polarized antennas benefit from receiving signals in any direction, are immune to interference, and are effective in fading environments [1]. Mobile communication is growing fast due to technological advancements as users increase.

Broad bandwidth is required to accommodate more users. In such cases, wideband circularly polarized antennas are very much essential. Many techniques are adopted to improve the axial ratio bandwidth of CP antenna [2–5]. The wide bandwidth is obtained using a monopole antenna with partial ground plane [2], microstrip patch antenna with multiple modes [3], slot loaded with strip [4], and stub loading methods [5]. In [6], a 'C' shaped slot with a sword-shaped radiator is used to obtain wide CP bandwidth. A G-shaped grounded ring slot is proposed in [7] to achieve wideband CP with an asymmetric ground plane. The patch antenna is designed to achieve wideband CP using combined TM modes and shorting pins in [8] and multimode resonances in [9]. A strip-based excitation technique is proposed in [10] to achieve broadband CP. Dual wideband CP is obtained using a modified monopole antenna in [11]. A two-element patch antenna with a circular reflector is used to obtain wideband CP [12]. In [13], wideband CP is proposed for implantable applications using a corner truncated patch antenna with strip loading. The above designs use the conventional methods of varying structural dimensions to achieve wide axial ratio bandwidth. Nowadays metametrials and their two

Received 7 February 2023, Accepted 29 April 2023, Scheduled 16 May 2023
* Corresponding author: Punneth Kumar Tharehalli Rajanna (punithkumartr@sit.ac.in).
[1] Department of Electronics and Telecommunication, Siddaganga Institute of Technology, BH Road, Tumkur 572103, India.
[2] Department of Electronics and Communication, National Institute of Technology Karnataka, Surathkal 575025, India.
[3] MEAD, Space Application Center, Indian Space Research Organization, Ahemedabad, India.

dimensional derivatives such as metasurfaces have potential applications such as sensors [14], filters [15], beam steering and beam reconfigurability [16, 17], time delay equalizer for EBG resonator [18], and environment sensing applications [19]. Also, the antennas are designed using metasurfaces to achieve wideband CP in combination with primary sources [20–25]. Frequency selective surface (FSS)-based reflective metasurfaces are used in [26–29] to obtain wide CP bandwidth and gain enhancement. Polarization conversion metasurfaces in [30–33] are used to convert linearly polarized waves to circularly polarized waves with good axial ratio bandwidths. The above discussed metasurfaces are fabricated as printed layers. The elements in a few metasurfaces are also fabricated using dielectric material (called as dielectric metasurfaces) [34, 35] or all metal [36] patches, which are application specific. The inference from the above designs is that the axial ratio is achieved with much effort, complex feeding techniques, and more strip loading methods. Also, the frequency of operation of the designs is approximately above 3 GHz. Much effort is needed to achieve axial ratio in the lower frequency range, like L and S bands, and these methods require more optimization time of the parameters used in the design.

The proposed method uses a simple CPW-fed monopole antenna with an asymmetric ground plane and a modified slot structure to obtain the wideband CP in the lower frequency range. The gain is enhanced using a phase gradient reflective metasurface. To get wideband CP, the CPW-fed monopole with the asymmetric ground plane gives CP in the lower frequencies, and the modified slot structure with two asymmetric strips introduced gives CP in the upper frequencies. The combined axial ratio points of the monopole mode and modes in the modified slot structure provide wider axial ratio bandwidth. However, the gain of the monopole design was less and improved using phase gradient metasurface (PGM). The proposed antenna has a -10 dB impedance bandwidth of 0.98 GHz to 2.77 GHz. The axial ratio is preserved over a frequency band of 1.4 GHz to 2.83 GHz.

2. GEOMETRY AND OPERATING PRINCIPLE

2.1. Antenna Geometry

The proposed design consists of a monopole with an asymmetric ground plane etched on the top side and a slot with rectangular strips etched at the bottom side of the FR4 ($\epsilon_r = 4.3$, $\tan\delta = 0.025$) substrate with a height of 1.6 mm. The proposed antenna is designed to operate in the microwave frequency range from 0.97 GHz to 2.77 GHz. A CPW feeding technique is used to excite the antenna. PGM is placed below the monopole antenna to improve the antenna's gain. The PGM consists of 6×6 unit cells, which are square-shaped etched on the top surface of the Rogers substrate ($\epsilon_r = 3.38$, $\tan\delta = 0.009$) with

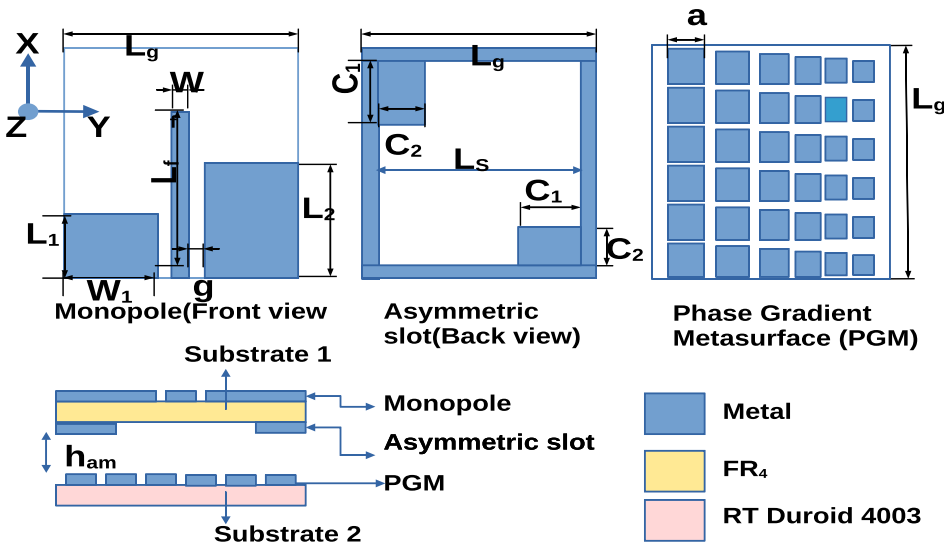

Figure 1. Antenna geometry ($L_g = 120$ mm, $W_f = 3.5$ mm, $L_f = 89$ mm, $W_1 = 58.05$ mm, $L_1 = 28$ mm, $L_2 = 53$ mm, $C_1 = 33$ mm, $C_2 = 26$ mm, $L_s = 100$ mm, $a = 19.9$ mm, $ham = 40$ mm).

a thickness of 6.35 mm. The unit cells are gradually varied to achieve multiple zero reflection phase points. The proposed design is shown in Fig. 1. The square unit cell of dimension 19.9 mm × 19.9 mm gives a reflection phase at a frequency of 1.27 GHz. The gradual decrease in the unit cell dimensions will produce multiple zero reflection phases, which helps to achieve stable gain over a wide operating band.

2.2. Operating Principle

In the proposed design, circular polarization is achieved over the wide operating bandwidth. The monopole antenna is designed to operate in lower frequencies. The monopole dimension is chosen based on the resonant frequency given by Equation (1). The ground plane in the traditional monopole antenna has equal dimensions in the CPW feeding, so it is difficult to generate CP radiation due to horizontal currents which are in opposite phases. This is shown in Fig. 2(a). From the figure, it is observed that the current distributions in the horizontal direction of the CPW ground plane are in opposite directions. Therefore, the horizontal currents are in opposite phases and cancel each other, and vertical fields are produced. Due to this, the radiation obtained is purely linear polarization, and axial ratio value over

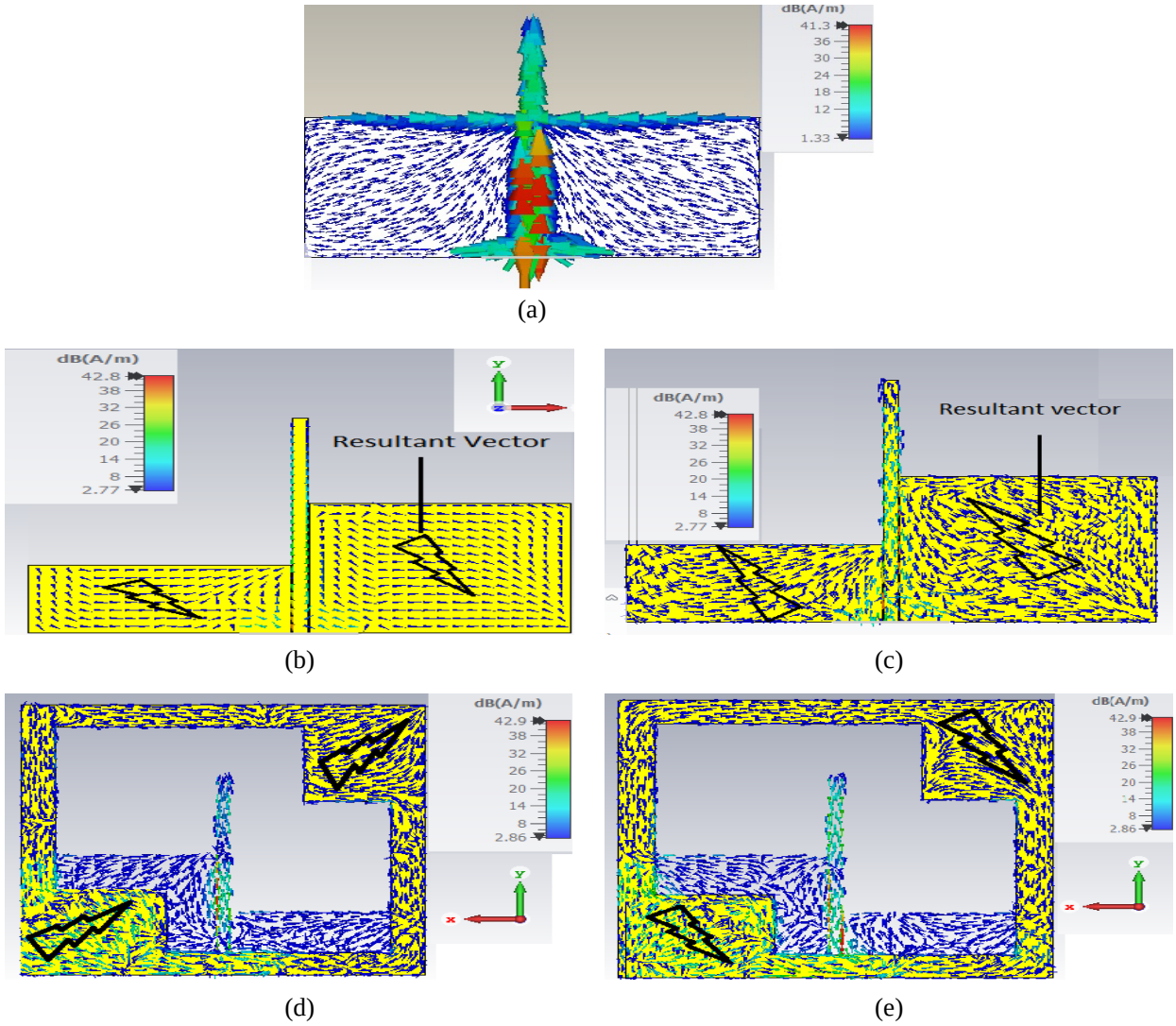

Figure 2. (a) Surface current distribution of traditional monopole. Surface current distribution at 1.5 GHz, (b) $\omega t = 0°$, (c) $\omega t = 90°$ and at 2.4 GHz, (d) $\omega t = 0°$, (e) $\omega t = 90°$.

the bandwidth is too large, which is shown in Fig. 4(b). The circular polarization is achieved by exciting two orthogonal modes with equal amplitude and 90° phase difference. This is achieved by adopting the asymmetric ground plane. The horizontal and vertical currents produce CP in the monopole [37]. To verify this, the rotation of surface currents at 1.7 GHz is captured at different time instances, shown in Figs. 2(b) and 2(c). It is observed from the figure that vectors rotate in the anticlockwise direction (w.r.t $+z$-direction). This indicates that the antenna produces right-hand circular polarization (RHCP) due to the asymmetric ground plane in the monopole. The slot is designed to operate at higher frequency using Equation (2). Since the slot structure is square, length and width are the same, and when it is excited it radiates the fundamental TM01 mode. Asymmetric strips are added to the slot antenna to produce two degenerative modes TM01 and TM10. These modes are excited with equal magnitude with orthogonal phase shift to produce CP. The asymmetry introduces orthogonal currents, which produce CP in the lower resonant frequency. The slot which contains rectangular strips is optimized to obtain CP in the upper resonant frequency. The surface current distributions at 1.5 GHz and 2.5 GHz of the proposed design are shown in Fig. 2. It is observed from the figure that vectors rotate in the anticlockwise direction (w.r.t $+z$-direction). This indicates that the antenna produces right-hand circular polarization (RHCP) due to the asymmetric ground plane as shown in Fig. 2(b) and Fig. 2(c). Similarly, in Figs. 2(d) and 2(e), the vectors rotate clockwise in the $-z$-direction producing RHCP due to asymmetry in the slot structure. The combined modes from the slot and monopole produce wideband CP operation. The axial ratio is optimized to obtain wideband circular polarization in the frequency range of 1.4 GHz to 2.83 GHz. The design stages of the proposed antenna geometry are shown in Fig. 3.

$$l = \frac{c}{4f\sqrt{\epsilon_{eff}}} \tag{1}$$

$$f = \frac{c}{2L_S}\sqrt{\frac{2}{\epsilon_r + 1}} \tag{2}$$

The reflection coefficient and axial ratio plots of the design steps are shown in Fig. 4(a) and Fig. 4(b). In Figure 3, stage 1 shows the design of a monopole, which has only the top layer with a symmetric ground plane. It gives the resonance frequency at 1.7 GHz, as shown in Fig. 3, but the impedance matching is poor. Also, the axial ratio value is 40, which gives purely linear polarization. In stage 2,

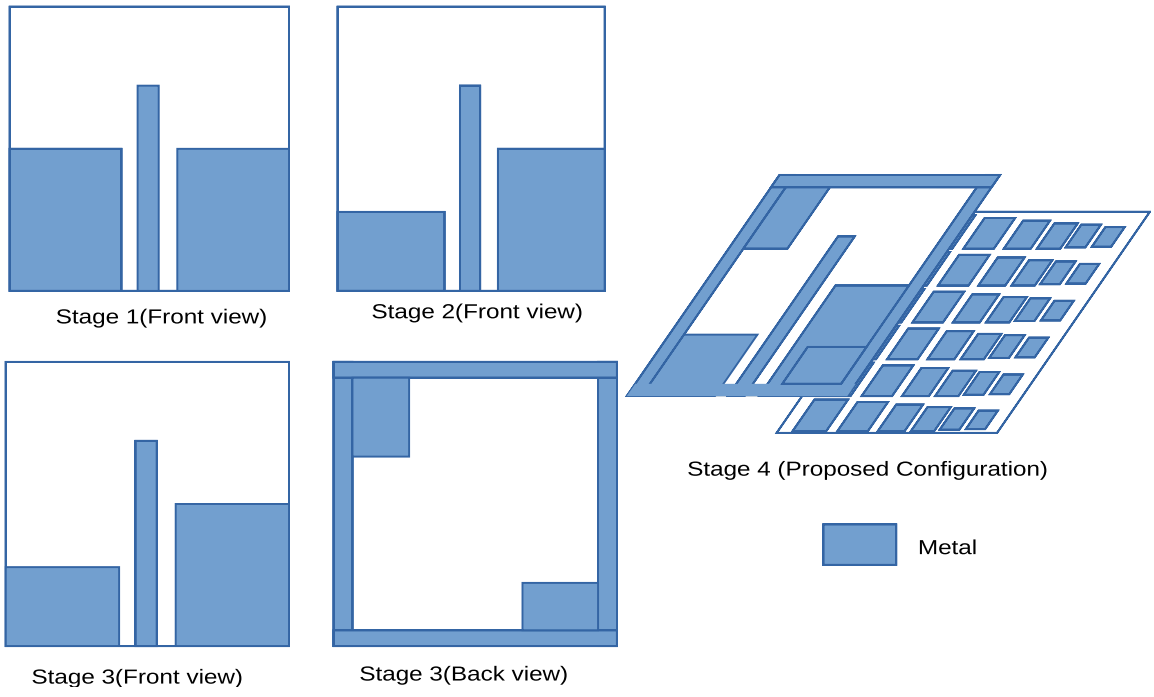

Figure 3. Geometry of antenna design steps.

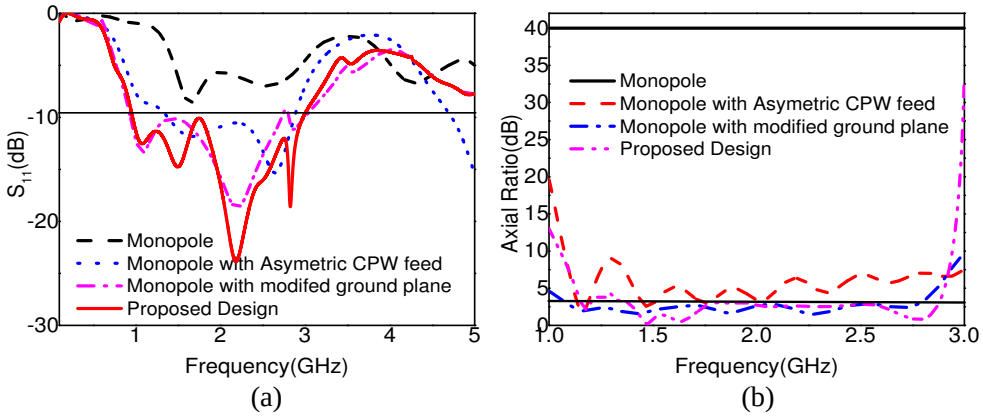

Figure 4. (a) Reflection coefficient of the antenna design steps. (b) Axial ratio of the antenna design steps.

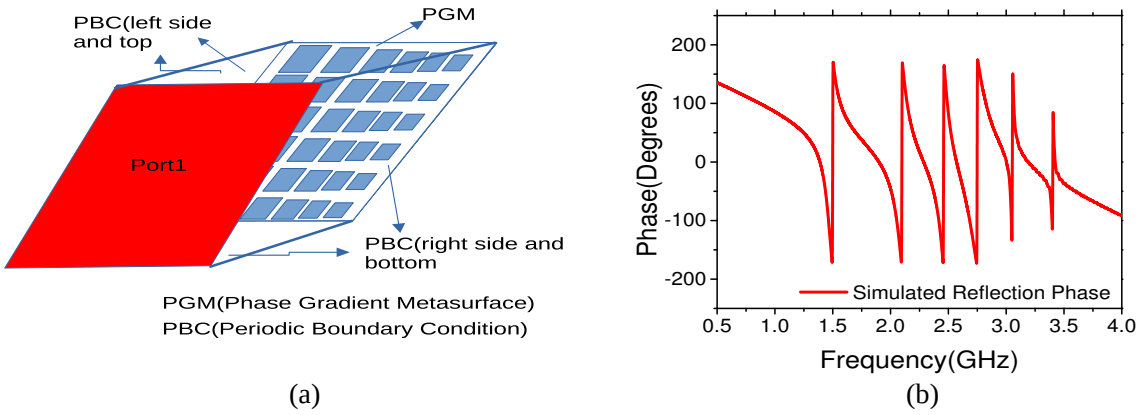

Figure 5. (a) Simulation setup of PGM. (b) Reflection phase characteristics of PG.

The asymmetric CPW feeding will provide the CP characteristics at 1.5 and 1.7 GHz with < 3 dB axial ratio values. This occurs when orthogonal currents of horizontal and vertical currents produced due to asymmetric ground plane. In stage 3, a slot is etched on the backside of monopole antenna with two rectangular strips introduced in the slot. The slot due to its asymmetric structure produces two degenerative modes required to obtain equal magnitude and 90° phase required for CP condition. The optimized values of these rectangular strips provide CP characteristics in the upper-frequency band. The combined resonances of slot and monopole produce CP over a wide bandwidth. At this stage, the gain is low over wideband due to the bidirectional radiation of the slot structure. A PGM is placed below the antenna to improve the gain value and radiate EM waves to the broadside. The PGM is sub-wavelength patches, and the dimensions are taken as one by tenth of λ, where λ is the free space wavelength. Basically, a square unit cell is designed in the initial stage, and PGM is obtained by gradual variation of basic square unit cell with 10% reduction in dimension. This can be reduced according to the required zero reflection phase points. A gradual variation of this square unit cell will produce multiple reflection phase characteristics. The PGM contains 6×6 unit cells, which is simulated with perfect electric conductor (PEC) in the bottom side of the unit cell and periodic boundary condition for sidewalls as shown in Fig. 5(a). The gradual variation of the unit cell dimension will produce the zero reflection phase points at multiple frequencies. This zero phase reflection point reflects the waves which are coming to the PGM back to forward direction with zero phase variations. In the conventional metasurfaces without phase gradient condition, it will produce only single zero reflection point, which enhances the gain at that frequency point. The phase gradient metasurface has nearby multiple zero

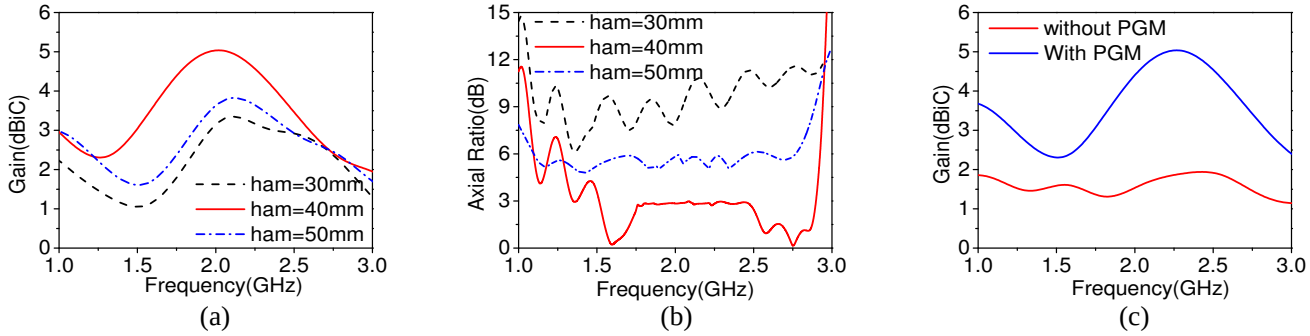

Figure 6. (a) Gain and (b) axial ratio variation of proposed antenna for different height between the monopole and PG. (c) Gain of the proposed design with and without PGM.

reflection points which are produced to increase the gain over wider bandwidth. The reflection phase characteristic is shown in Fig. 5(b). The height between monopole antenna and PGM is optimized to get stable gain over a wide operating band at the cost of little axial ratio deterioration in the lower frequency. The height of PGM from the primary antenna is optimized to obtain good gain and axial ratio values. Gain and axial ratio variations of the proposed design for different heights between PGM and monopole are shown in Fig. 6(a) and Fig. 6(b). From the figures, it is seen that the gain and axial ratio are sensitive to the height. When the height is increased or decreased beyond the optimum height, and gain and axial ratios are deteriorated due to phase variations of two combined slot and monopole modes. Gain enhancement of the proposed design with and without PGM is shown in Fig. 6(c). The gain without PGM is low, around 1.8 dBic, and it is improved after introducing PGM at an optimum height.

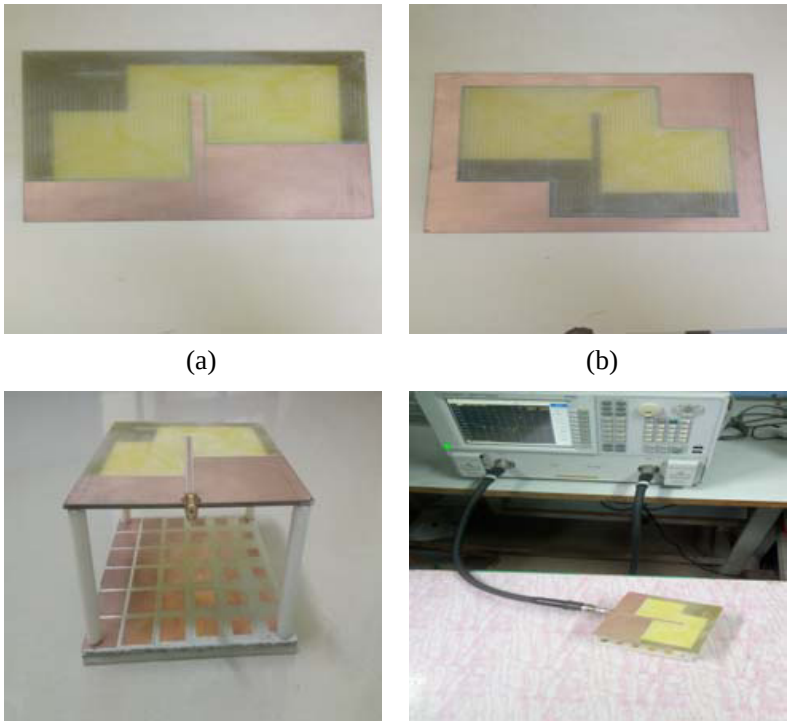

Figure 7. Prototype of the fabricated structure. (a) Front view. (b) Back view. (c) Proposed design. (d) Measurement set-up.

3. EXPERIMENTAL RESULTS AND DISCUSSION

The fabricated prototype of the wideband CP antenna is shown in Fig. 7. Spacers separate the monopole and PGM at an optimized height for better performance. The simulated impedance bandwidth (< -10 dB) of 98.96% (0.98 GHz–2.9 GHz) and measured impedance bandwidth of 95.46% (0.98 GHz–2.77 GHz) are obtained, and they are shown in Fig. 8(a). Fig. 8(b) gives the measured and simulated axial ratio bandwidths of 67.61% (1.4 GHz–2.83 GHz). The peak gain of 5.2 dBic is noted at 2.35 GHz. The measured and simulated gains are in good agreement with 2 dB variations over the entire bandwidth, which is depicted in Fig. 8(c). This is due to variations of multiple reflection phase characteristics of PGM. The simulated radiation efficiency of above 50% is noted in the entire bandwidth and is shown in Fig. 8(d). The simulated results are compared with the measured results of the radiation patterns

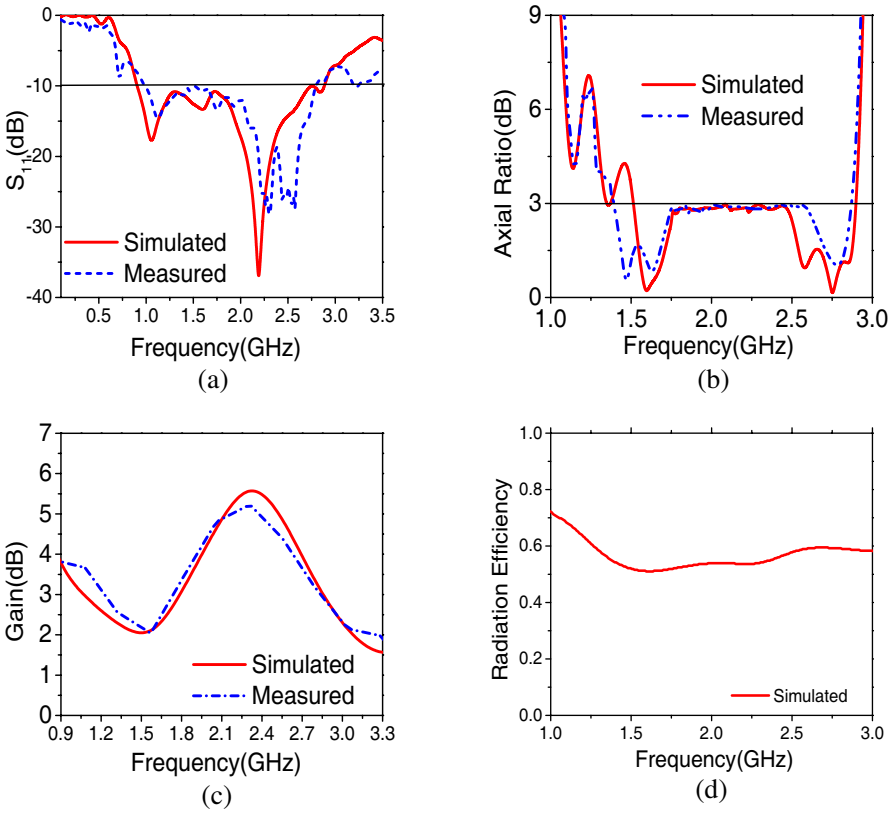

Figure 8. Simulated and measured (a) S_{11} (dB). (b) Axial ratio (dB). (c) Gain. (d) Simulated radiation efficiency.

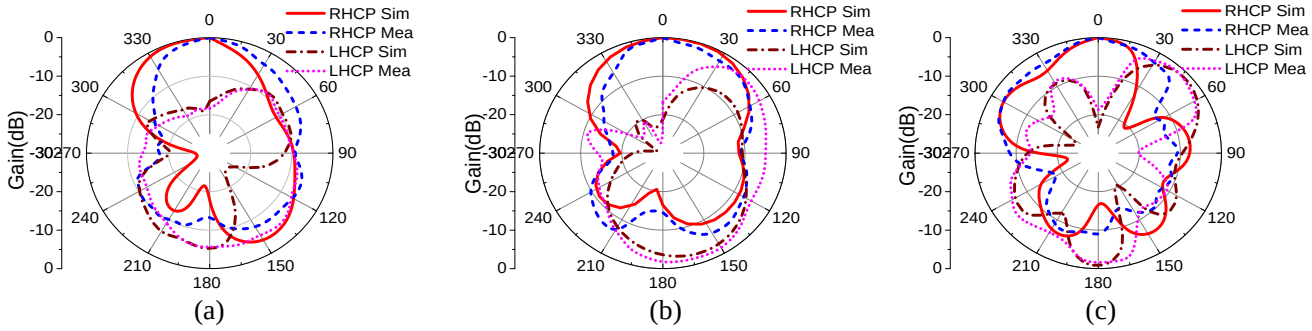

Figure 9. Simulated and measured radiation patterns at (a) 1.46 GHz, (b) 1.63 GHz, (c) 2.78 GHz.

at three distinct frequencies over the entire bandwidth to ensure that the antenna radiates circularly polarized wave. The radiation patterns at 1.46 GHz, 1.63 GHz, and 2.6 GHz are shown in Figs. 9(a), 9(b), and 9(c), respectively. The proposed wideband antenna will radiate RHCP in the broadside direction. The Left-hand circular polarization (LHCP) is the cross-polar component, and a minimum of −15 dB is achieved within the obtained axial ratio bandwidth. Table 1 shows the comparison of previous works with the proposed work. The proposed work achieved better performance than some of the works in terms of impedance bandwidth, axial ratio bandwidth, and size of the antenna geometry.

Table 1. Comparison of previous work with proposed design.

Reference	size	Antenna Profile	Impedance bandwidth	Axial ratio bandwidth	Peak gain (dBic)
[7]	$0.57\lambda_0 \times 0.57\lambda_0$	–	109%	95%	3
[9]	$0.3\lambda_0 \times 0.28\lambda_0$	–	72%	66%	6.3
[10]	$1.46\lambda_0 \times 1.46\lambda_0$	–	111%	55%, 29.3%	4.2, 3.4
[11]	$1.91\lambda_0 \times 1.91\lambda_0$	$0.26\lambda_0$	83%	49%	8.6
[20]	$0.66\lambda_0 \times 0.66\lambda_0$	–	43%	22%	6.6
[24]	$1.5\lambda_0 \times 1.5\lambda_0$	$0.51\lambda_0$	64%	18%	12.88
[25]	$0.46\lambda_0 \times 0.46\lambda_0$	–	29.7%	21.4%	5.6
[27]	$1.17\lambda_0 \times 1.32\lambda_0$	$0.31\lambda_0$	63.22%	31.14%	5
[29]	$0.47\lambda_0 \times 0.47\lambda_0$	$0.23\lambda_0$	100%	58.15%	9
[PW]	$0.75\lambda_0 \times 0.75\lambda_0$	$0.28\lambda_0$	95.46%	67.61%	5.2

* λ_0 = Free space wavelength, PW = Proposed work

4. CONCLUSIONS

A wideband antenna with circular polarization characteristics is successfully designed and fabricated. A CPW-fed monopole antenna with an asymmetric ground plane and a slot structure with asymmetric rectangular strips are designed to obtain broadband circular polarization characteristics. The monopole provides good axial ratio bandwidth in the lower frequencies. The slot with asymmetric rectangular strips is introduced to achieve a better axial ratio bandwidth at higher frequencies. The gain is enhanced using the phase gradient metasurface. The proposed design is fabricated and measured. The experimental results are in good agreement with the simulated ones. Wide axial ratio bandwidth of 67.61% is obtained in L and S bands. The proposed design is well suitable for L and S-band radar and satellite applications where CP is the essential requirement.

ACKNOWLEDGMENT

We thank the Rogers corporation for providing substrate materials to fabricate the proposed antenna.

REFERENCES

1. Gao, S. S., Q. Luo, and F. Zhu, *Circularly Polarized Antennas*, Wiley, IEEE Press, Nov. 2013.
2. Samsuzzaman, M., M. T. Islam, and M. J. Singh, "A compact printed monopole antenna with wideband circular polarization," *IEEE Access*, Vol. 6, 54713–54725, 2018, doi: 10.1109/ACCESS.2018.2871818.
3. Wang, L. and Y.-F. En, "A wideband circularly polarized microstrip antenna with multiple modes," *IEEE Open Journal of Antennas and Propagation*, Vol. 1, 413–418, 2020, doi: 10.1109/OJAP.2020.3009884.

4. Ullah, U. and S. Koziel, "A broadband circularly polarized wide-slot antenna with a miniaturized footprint," *IEEE Antennas and Wireless Propagation Letters*, Vol. 17, No. 12, 2454–2458, Dec. 2018, doi: 10.1109/LAWP.2018.2877800.
5. Birwal, A., S. Singh, B. Kanaujia, and S. Kumar, "Broadband CPW-fed circularly polarized antenna for IoT-based navigation system," *International Journal of Microwave and Wireless Technologies*, Vol. 11, No. 8, 835–843, 2019, doi: 10.1017/S1759078719000461.
6. Xu, R., J.-Y. Li, and J. Liu, "A design of broadband circularly polarized C-shaped slot antenna with sword-shaped radiator and its array for L/S-band applications," *IEEE Access*, Vol. 6, 5891–5896, 2018, doi: 10.1109/ACCESS.2017.2788008.
7. Liang, C.-F., Y.-P. Lyu, D. Chen, W. Zhang, and C.-H. Cheng, "A low-profile and wideband circularly polarized patch antenna based on TM11 and TM21," *IEEE Transactions on Antennas and Propagation*, Vol. 69, No. 8, 4439–4446, Aug. 2021, doi: 10.1109/TAP.2020.3049007.
8. Saraswat, K., T. Kumar, and A. Harish, "A corrugated G-shaped grounded ring slot antenna for wideband circular polarization," *International Journal of Microwave and Wireless Technologies*, Vol. 12, No. 5, 431–436, 2020, doi: 10.1017/S1759078719001624.
9. Ullah, U. and S. Koziel, "A novel coplanar-strip-based excitation technique for design of broadband circularly polarization antennas with wide 3 dB axial ratio beamwidth," *IEEE Transactions on Antennas and Propagation*, Vol. 67, No. 6, 4224–4229, Jun. 2019, doi: 10.1109/TAP.2019.2908114.
10. Xu, R., J.-Y. Li, J. Liu, S.-G. Zhou, and K. Wei, "A simple design of compact dual-wideband square slot antenna with dual-sense circularly polarized radiation for WLAN/Wi-Fi communications," *IEEE Transactions on Antennas and Propagation*, Vol. 66, No. 9, 4884–4889, Sept. 2018, doi: 10.1109/TAP.2018.2851671.
11. Mcpherson, T. J., Z. Iqbal, and S. Lim, "A wideband, circularly polarized, directive antenna with a circular reflector," *IEEE Access*, Vol. 7, 177703–177712, 2019, doi: 10.1109/ACCESS.2019.2958528.
12. Hu, W., C. Li, L. Wen, et al., "Wideband circularly polarized microstrip patch antenna with multimode resonance," *IEEE Antennas and Wireless Propagation Letters*, Vol. 20, No. 4, 533–537, Apr. 2021, doi: 10.1109/LAWP.2021.3056404.
13. Yang, Z., L. Zhu, and S. Xiao, "An implantable wideband circularly polarized microstrip patch antenna via two pairs of degenerate modes," *IEEE Access*, Vol. 7, 4239–4247, 2019, doi: 10.1109/ACCESS.2018.2887234.
14. Esfandiyari, M., A. Lalbakhsh, S. Jarchi, M. Ghaffari-Miab, H. Noori Mahtaj, and R. B. V. B. Simorangkir, "Tunable terahertz filter/antenna-sensor using graphene-based metamaterials," *Materials & Design*, Vol. 220, 110855, 2022, doi: 10.1016/j.matdes.2022.110855.
15. Lalbakhsh, A., M. U. Afzal, K. P. Esselle, and S. L. Smith, "All-metal wideband frequency-selective surface bandpass filter for TE and TM polarizations," *IEEE Transactions on Antennas and Propagation*, Vol. 70, No. 4, 2790–2800, Apr. 2022, doi: 10.1109/TAP.2021.3138256.
16. Das, P., K. Mandal, and A. Lalbakhsh, "Beam-steering of microstrip antenna using single-layer FSS based phase-shifting surface," *Int. J. RF Microw. Comput. Aided Eng.*, Vol. 32, No. 3, e23033, 2022, doi: 10.1002/mmce.23033.
17. Das, P., K. Mandal, and A. Lalbakhsh, "Single-layer polarization-insensitive frequency selective surface for beam reconfigurability of monopole antennas," *Journal of Electromagnetic Waves and Applications*, Vol. 34, No. 1, 86–102, 2020.
18. Lalbakhsh, A., M. U. Afzal, and K. P. Esselle, "Multiobjective particle swarm optimization to design a time-delay equalizer metasurface for an electromagnetic band-gap resonator antenna," *IEEE Antennas and Wireless Propagation Letters*, Vol. 16, 912–915, 2017, doi: 10.1109/LAWP.2016.2614498.
19. Lalbakhsh, A., R. B. V. B. Simorangkir, N. Bayat-Makou, A. Kishk, and K. Esselle, "Advancements and artificial intelligence approaches in antennas for environmental sensing," *Artificial Intelligence and Data Science in Environmental Sensing*, 1st Edition, Chapter 2, 19–38, Elsevier, 2022, doi: 10.1016/B978-0-323-90508-4.00004-6.

20. Supreeyatitikul, N., T. Lertwiriyaprapa, and C. Phongcharoenpanich, "S-shaped metasurface-based wideband circularly polarized patch antenna for C-band applications," *IEEE Access*, Vol. 9, 23944–23955, 2021, doi: 10.1109/ACCESS.2021.3056485.
21. Zarbakhsh, S., M. Akbari, F. Samadi, and A. Sebak, "Broadband and high-gain circularly-polarized antenna with low RCS," *IEEE Transactions on Antennas and Propagation*, Vol. 67, No. 1, 16–23, Jan. 2019, doi: 10.1109/TAP.2018.2876234.
22. Tran, H. H., C. D. Bui, N. Nguyen-Trong, and T. K. Nguyen, "A wideband non-uniform metasurface-based circularly polarized reconfigurable antenna," *IEEE Access*, Vol. 9, 42325–42332, 2021, doi: 10.1109/ACCESS.2021.3066182.
23. Liu, Z., Y. Liu, and S. Gong, "Gain enhanced circularly polarized antenna with RCS reduction based on metasurface," *IEEE Access*, Vol. 6, 46856–46862, 2018, doi: 10.1109/ACCESS.2018.2865533.
24. Supreeyatitikul, N., A. Boonpoonga, and C. Phongcharoenpanich, "Z-shaped metasurface-based wideband circularly polarized Fabry-Pérot antenna for C-band satellite technology," *IEEE Access*, Vol. 10, 59428–59441, 2022.
25. Zheng, B., N. Li, X. Li, X. Rao, and Y. Shan, "Miniaturized wideband CP antenna using hybrid embedded metasurface structure," *IEEE Access*, Vol. 10, 120056–120062, 2022, doi: 10.1109/ACCESS.2022.3221825.
26. Zheng, Q., C. Guo, and J. Ding, "Wideband metasurface-based reflective polarization converter for linear-to-linear and linear-to-circular polarization conversion," *IEEE Antennas and Wireless Propagation Letters*, Vol. 17, No. 8, 1459–1463, Aug. 2018, doi: 10.1109/LAWP.2018.2849352.
27. Rajanna, P. K. T., K. Rudramuni, and K. Kandasamy, "A wideband circularly polarized slot antenna backed by a frequency selective surface," *Journal of Electromagnetic Engineering Sciences*, Vol. 19, No. 3, 166–171, 2019.
28. Sharma, A., et al., "Wideband high-gain circularly-polarized low RCS dipole antenna with a frequency selective surface," *IEEE Access*, Vol. 7, 156592–156602, 2019, doi: 10.1109/ACCESS.2019.2948176.
29. Adibi, S., M. A. Honarvar, and A. Lalbakhsh, "Gain enhancement of wideband circularly polarized UWB antenna using FSS," *Radio Science*, Vol. 56, e2020RS007098, 2021, https://doi.org/10.1029/2020RS007098.
30. Li, K., Y. Liu, Y. Jia, and Y. J. Guo, "A circularly polarized high-gain antenna with low RCS over a wideband using chessboard polarization conversion metasurfaces," *IEEE Transactions on Antennas and Propagation*, Vol. 65, No. 8, 4288–4292, Aug. 2017, doi: 10.1109/TAP.2017.2710231.
31. Chen, Q. and H. Zhang, "Dual-patch polarization conversion metasurface-based wideband circular polarization slot antenna," *IEEE Access*, Vol. 6, 74772–74777, 2018, doi: 10.1109/ACCESS.2018.2883992.
32. Rajanna, P., K. Rudramuni, and K. Kandasamy, "Characteristic mode-based compact circularly polarized metasurface antenna for in-band RCS reduction," *International Journal of Microwave and Wireless Technologies*, Vol. 12, No. 2, 131–137, 2020, doi: 10.1017/S1759078719001119.
33. Genovesi, S. and F. A. Dicandia, "Characteristic modes analysis of a near-field polarization-conversion metasurface for the design of a wideband circularly polarized X-band antenna," *IEEE Access*, Vol. 10, 88932–88940, 2022, doi: 10.1109/ACCESS.2022.3200303.
34. Lalbakhsh, A., M. U. Afzal, K. P. Esselle, S. L. Smith, and B. A. Zeb, "Single-dielectric wideband partially reflecting surface with variable reflection components for realization of a compact high-gain resonant cavity antenna," *IEEE Transactions on Antennas and Propagation*, Vol. 67, No. 3, 1916–1921, Mar. 2019, doi: 10.1109/TAP.2019.2891232.
35. Young, S. M., M. Kauf, J. Kutsch, and A. Grbic, "Additively-manufactured all-dielectric microwave polarization converters using ceramic stereolithography," *IEEE Open Journal of Antennas and Propagation*, Vol. 4, 339–348, 2023, doi: 10.1109/OJAP.2023.3257355.
36. Lalbakhsh, A., M. U. Afzal, T. Hayat, et al., "All-metal wideband metasurface for near-field transformation of medium-to-high gain electromagnetic sources," *Sci. Rep.*, Vol. 11, 9421, 2021, https://doi.org/10.1038/s41598-021-88547-3.

37. Ding, K., Y.-X. Guo, and C. Gao, "CPW-fed wideband circularly polarized printed monopole antenna with open loop and asymmetric ground plane," *IEEE Antennas and Wireless Propagation Letters*, Vol. 16, 833–836, 2017, doi: 10.1109/LAWP.2016.2606557.